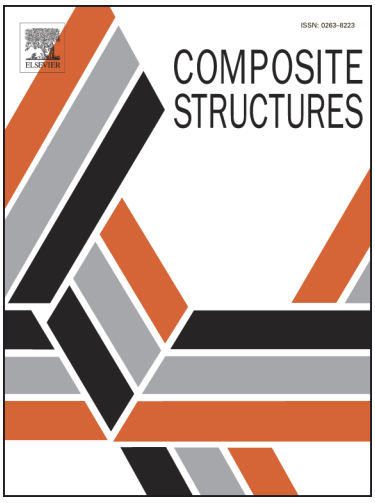

A New Sandwich Element for Modeling of Partially Delaminated Sandwich Beam Structures

A.R. Damanpack, M. Bodaghi

PII: S0263-8223(20)32994-9
DOI: https://doi.org/10.1016/j.compstruct.2020.113068
Reference: COST 113068

To appear in: *Composite Structures*

Received Date: 15 July 2020
Revised Date: 22 September 2020
Accepted Date: 28 September 2020

Please cite this article as: Damanpack, A.R., Bodaghi, M., A New Sandwich Element for Modeling of Partially Delaminated Sandwich Beam Structures, *Composite Structures* (2020), doi: https://doi.org/10.1016/j.compstruct.2020.113068

A New Sandwich Element for Modeling of Partially Delaminated Sandwich Beam Structures

A.R. Damanpack[a†] and M. Bodaghi[b]

[a] *Department of Technology and Innovation, University of Southern Denmark, Odense, Denmark*

[b] *Department of Engineering, School of Science and Technology, Nottingham Trent University, Nottingham NG11 8NS, United Kingdom*

Abstract

In this paper, a new sandwich beam element is introduced for analyzing sandwich beam structures with a flexible core and partially delaminated regions. In this element, interfaces between the core and face sheets are modeled by two independent layers. The model uses a high-order sandwich panel theory to consider flexibility of the core with nonlinearities associated with geometry and real contact characteristics of the delaminated regions. The proposed motion field takes advantage of both displacement and displacement gradients in the core boundaries. Therefore, the kinematics allow continuity conditions for displacements and rotations at the interfaces to be exactly satisfied in fully bounded and delamination regions. By using finite element (FE) formulation with Hermite shape functions, elemental vectors and matrices are derived in the framework of Hamilton's principle. FE governing equations are solved by Newton-Raphson iterative scheme. A 2D FE method is also developed to verify predictions of the sandwich model for various delamination cases. Comparison studies show that results from both sandwich and 2D FE models are in a good agreement. They can predict large-deformation results for the sandwich behaviors much better than the simplified model available in the literature. A set of parametric study is devoted to provide an insight into the influence of boundary condition, number and position of delaminated regions on deformations, stresses and instability of fully clamped and cantilever sandwich beams. The developed formulation is not only more computationally efficient than 2D models usually used for such analysis, but also at the same time is accurate, simple and robust. It is also found that modeling of the delaminated zone core and stress distribution at each interface independently is crucial to accurately analyze instability behaviors of sandwich structures.

Keywords: *Partial delamination, High-order, Nonlinearity, Contact, Sandwich beam, Finite element method.*

[†] Corresponding Author
Tel.: +45 6550 9470; *E-mail address:* adpm@sdu.dk

1. Introduction

In various industries, sandwich structures are broadly employed as key elements with low weight, high strength and stiffness. Modern sandwich structures consist of two stiff metallic or composite thin face sheets bonded to a soft/stiff honeycomb or foam core of low/high density. A simple model used for honeycomb core sandwich panels was introduced as a classical sandwich panel theory by Di Taranto [1]. This model considered that the top and the bottom face sheets of the sandwich beam deform based on the Bernoulli–Euler beam theory, whereas the core only experiences a shear deformation. Khalili et al. [2] used polymer foam materials as core of sandwich structures that required application of an advanced theory for the vertical flexibility feature. In this respect, Frostig [3] presented a new model for sandwich beams to analyze both fully bonded and delaminated sandwich structures with a flexible core based on the high-order theory. In this model, axial and transverse displacements for the core were considered with two and three order polynomials, respectively. Comparing their predictions with experiments and those obtained by the classical formulation showed superiority of the high-order formulation. Many research works have been done based on the high-order sandwich panel theory. Linke et al. [4] presented a sandwich element for the stability analysis of sandwich panels considering the high-order theory. Using second and third order polynomials for the displacement field of the core is known as extended high-order sandwich theory used in many researches. For example, Bekuit et al. [5] developed a quasi two-dimensional finite element (FE) formulation for the static and dynamic analyses of sandwich beams. The through-the-thickness variation of each displacement field in each layer was expanded in polynomials and the span-wise variation was interpolated using Lagrange cubic shape functions. Phan et al. [6, 7] and Frostig et al. [8] used the extended high-order theory for the analysis of sandwich beams under wrinkling, global buckling and free vibration. Elmalich and Rabinovitch [9, 10] developed the high-order FE models of multi-layer soft-core sandwich plates with/without geometrical nonlinearity. Comparing the results with experiments showed the high accuracy of the high-order theory and the significant effect of the geometrical nonlinearity on the structure responses. Kheirikhah et al. [11] improved the high-order sandwich plate theory by assuming the third-order plate theory for face sheets and quadratic and cubic functions for transverse and in-plane displacements of the core. In this theory, the continuity conditions for transverse shear stresses at the interfaces as well as the conditions of zero transverse shear stresses on the upper and lower surfaces of the plate were satisfied. Damanpack et al. introduced two different types of sandwich beam elements consisting of three [12] and five [13] layers. The FE formulation was derived based on the high-order sandwich beam theory for low velocity and nonlinear active control analyses. Magnucki et al. [14] performed a buckling analysis of a five-layer sandwich beam by using the FE method. The main purpose of research was to present an analytical model for the five-layer beam and to compare the results from theoretical, numerical and experimental analyses.

Frostig and Sokolinsky [15] carried out a nonlinear static analysis of delaminated sandwich beams using the high-order theory. In this case, the contact conditions were considered constant

regardless of the response of the structure. Frostig et al. [16, 17] developed a high-order theory of sandwich panels considering geometrical non-linearity for face sheet layers and the core. In this model, face sheets deform based on the Bernoulli–Euler beam theory by considering large displacements and moderate rotations. The field of equations for the core was proposed in two different approaches. The axial stress was neglected in both cases and the distribution of vertical normal stress through the depth of the core was assumed to be linear. In the first formulation, moderate rotations were considered for the core shear strain (von Karmann class of deformations) while the deformation was assumed to be linear in the second case. The numerical results were compared and verified by the results from commercial codes ADINA and ANSYS for three-point bending.

The second approach was used by Frostig and Thomsen [18] to analyze delaminated sandwich panels under bending. The core with a delaminated zone was assumed to be free of shear stresses while constant compressive stresses were considered during the contact. Contact occurred only when the vertical normal stress was negative at the debonded interface. No contact condition was also applied mathematically by setting a zero value for modulus of elasticity of the core during positive vertical normal stresses. Schwarts-Givli et al. [19] used the high-order theory for the nonlinear dynamic analysis of delaminated sandwich structures. A general analytical model was proposed for the contact features of the delaminated interface. Frostig and Thomsen [20] and Frostig [21] adopted a high-order theory for the non-linear analysis of delaminated curved sandwich panels subjected to thermal and/or mechanical loadings. Kim and Choi [22] investigated the connection between layers of sandwich structures using a series of experimental programs. Experiments revealed that the shear resistance at interface layers was improved by the shear capacity of the shear plate besides the friction produced by the compressive force along the wall [23]. In a comprehensive study, Shokrieh and Heidari-Rarani [24] evaluated the effect of beam theories, foundation, material and crack properties on the first delamination mode in multidirectional laminated composites. Liu and Shu [25] presented an analytical solution to analyze the free vibration of rotating beams with multiple delaminations. In this study, both free and constrained modes were assumed in the delamination vibration. The effect of delamination and rotating speed on natural frequencies and corresponding shape modes were considered. Marjanovic and Vuksanovic [26] employed the layerwise plate theory of Reddy through an FE formulation to obtain natural frequencies, mode shapes and critical buckling loads for intact and damaged plates. Heaviside step functions were used for discontinuities in displacement field in three orthogonal directions. Another finite element modeling was proposed by McElroy et al. [27] for the analysis of the delamination-migration phenomena in laminate impact damage processes. The experimental data under a quasi-static indentation load were used to analyze transverse matrix crack and its grow on a new ply interface. Groh and Tessler [28] developed two different elements with 8 and 9 degree-of-freedom to escape shear locking phenomenon based on the zigzag theory of sandwich beams. These elements showed a good computational efficiency of predicting stresses in laminates with embedded delaminations. Pietrek and Horst [29] developed an FE model to simulate behaviors of sandwich cells with a delamination zone of face sheets under buckling loads.

The experimental tests showed significant effects of the failure loads and the delaminations size on the behaviors of adhesive layers. Kapuria and Ahmeda [30] extended a layerwise zigzag theory for the analysis of composite sandwich panels including multiple rebounding zones. The model neglected any flexibility through the thickness and the delaminated faces were assumed to have no mutual interaction during deformations. FE results showed a good agreement compared with three-dimensional FE solutions for delaminated composite plates under bending and free vibration.

The main aim of this study is to introduce a new sandwich element for the analysis of fully bonded or partially delaminated sandwich beam structures with a high accuracy. Independent interface layers between face sheets and core are considered to model adhesive materials and simulate the deboning zone. The high-order sandwich panel with flexible core is extended to take into account nonlinearities associated with geometry and real contact characteristics of the delaminated regions. The motion field is described with both displacement and strain functions in the core boundaries which allow continuity conditions for displacements and rotations at the interfaces to be exactly satisfied in fully bounded and delamination regions. FE formulation with Hermite shape functions is developed to extract elemental vectors and matrices using Hamilton's principle. Based on the FE model, a computational code is developed by computer programming in MATLAB® along with iterative Newton-Raphson scheme. On the other hand, a fully 2D FE method is also developed to verify and validate predictions of the presented sandwich model for various types of delamination problems. Comparative studies reveal that results from both sandwich and 2D FE models are in a good agreement. They can predict large-deformation results for the sandwich behaviors much better than the simplified model existing in the literature. Finally, numerical examples are presented in terms of deformations, stresses and instability to investigate effects of delamination parameters on the response of the sandwich structures in the small and large deformation ranges. The presented formulation and results are expected to contribute to a better understanding of the bending and local buckling behaviors of sandwich beams and to be instrumental towards an efficient design of sandwich beams with local delaminations.

2. Theory

2.1. Kinematic and constitutive equations

Fig. 1 shows a five-layer sandwich beam element with length l and width b. The Cartesian coordinate system is located on the mid-plane so that X-axis is along the beam length while Z-axis is through the bending direction and all deformations are considered in the XZ plane. It should be mentioned that theories of thin structures with small or moderate rotations such as Euler–Bernoulli may not be suitable for describing the behavior of face sheets due to localized bending effects induced in the delaminated region and vicinity of points of geometric and material discontinuities. Therefore, the top and bottom face sheets deform according to the first-order beam theory while a state of plane stress is assumed for the core. It is assumed that a material point moves along X and

Z directions equal to u and w. The displacement fields for each layer of sandwich beam element are defined as:

$$u:\begin{cases}\text{Top face sheet} & u_t(x,z) & |z-(h_c+h_t)/2| \le h_t/2\\ \text{Bottom face sheet} & u_b(x,z) & |z+(h_c+h_b)/2| \le h_b/2\\ \text{Core} & u_c(x,z,z^2,z^3) & |z| \le h_c/2\end{cases} \tag{1a}$$

$$w:\begin{cases}\text{Top face sheet} & w_t(x) & |z-(h_c+h_t)/2| \le h_t/2\\ \text{Bottom face sheet} & w_b(x) & |z+(h_c+h_b)/2| \le h_b/2\\ \text{Core} & w_c(x,z,z^2,z^3) & |z| \le h_c/2\end{cases} \tag{1b}$$

where h is the thickness and the sub-indices denote the layer name. The derivative of this field results in the Green-Lagrangian strain tensor $\boldsymbol{\epsilon}$ as:

$$\boldsymbol{\epsilon}:\begin{cases}\text{Face sheet:}\begin{cases}\epsilon_{xj}=u_{j,x}+\frac{1}{2}\left(u_{j,x}^2+w_{j,x}^2\right)\\ \gamma_j=u_{j,z}+w_{j,x}+u_{j,x}u_{j,z}\end{cases} & (j=t,b)\\ \text{core:}\begin{cases}\epsilon_{xc}=u_{c,x}+\frac{1}{2}\left(u_{c,x}^2+w_{c,x}^2\right)\\ \epsilon_{zc}=w_{c,z}+\frac{1}{2}\left(u_{c,z}^2+w_{c,z}^2\right)\\ \gamma_c=u_{c,z}+w_{c,x}+u_{c,x}u_{c,z}+w_{c,x}w_{c,z}\end{cases}\end{cases} \tag{2}$$

In this study, the sandwich panel consists of an orthotropic core integrated with two isotropic face sheets, where their plane stress constitutive equations based on the linear elastic material can be written as:

$$\boldsymbol{\sigma}:\begin{cases}\text{Face sheet:}\begin{cases}\sigma_{xj}=E_{xj}\varepsilon_{xj}\\ \tau_j=G_{zxj}\gamma_j\end{cases} & (j=t,b)\\ \text{core:}\begin{cases}\sigma_{xc}=Q_{xc}\varepsilon_{xc}+Q_c\varepsilon_{zc}\\ \sigma_{zc}=Q_{zc}\varepsilon_{zc}+Q_c\varepsilon_{xc}\\ \tau_c=G_{zxc}\gamma_c\end{cases}\end{cases} \tag{3}$$

where

$$Q_{xc}=\frac{E_{xc}}{(1-\frac{E_{xc}}{E_{zc}}\upsilon_{zxc}^2)},Q_{zc}=\frac{E_{zc}}{(1-\frac{E_{xc}}{E_{zc}}\upsilon_{zxc}^2)},Q_c=\frac{E_{xc}\upsilon_{zxc}}{(1-\frac{E_{xc}}{E_{zc}}\upsilon_{zxc}^2)} \tag{4}$$

and $\boldsymbol{\sigma}$ denotes the second Piola-Kirchhoff stress, E_{ij} is the Young's modulus along i-axis , G_{zij} is the shear modulus in direction of i-axis on the plane whose normal is in z direction, υ_{zxj} is the Poisson's ratio that corresponds to a contraction in the x direction when an extension is applied in the z direction and the j sub-indices denote the layer name. The elemental governing equation can be extracted by means of the Hamilton's principle as:

$$\int_{\bar{V}}(\delta U_{int}-\delta W_{ext})d\bar{V}=0 \tag{5}$$

where δU_{int} and δW_{ext} denote virtual internal (strain) energy and total virtual work done by external loads on the element. The integration is also applied over the domain of sandwich beam element. According to the proposed model, the virtual strain energy can be subdivided into three parts as:

$$\delta U_{int} = \int_{\bar{V}_t} (\sigma_{xt}\delta\varepsilon_{xt} + \tau_t\delta\gamma_t)dV_t + \int_{\bar{V}_b} (\sigma_{xb}\delta\varepsilon_{xb} + \tau_b\delta\gamma_b)dV_b + \int_{\bar{V}_c} (\sigma_{xc}\delta\varepsilon_{xc} + \sigma_{zc}\delta\varepsilon_{zc} + \tau_c\delta\gamma_c)dV_c \tag{6}$$

For the sandwich beam structures, the integration over the volume $\bar{V}$ can be expressed by the product of integration over the length and integration over the thickness as:

$$\begin{aligned}\delta U_{int} = b\int_0^l \Bigg(&\int_{\frac{h_c}{2}}^{\frac{h_c}{2}+h_t} (\sigma_{xt}\delta\varepsilon_{xt} + \tau_t\delta\gamma_t)dz + \int_{\frac{-h_c}{2}-h_b}^{\frac{-h_c}{2}} (\sigma_{xb}\delta\varepsilon_{xb} + \tau_b\delta\gamma_b)dz \\ &+ \int_{\frac{-h_c}{2}}^{\frac{h_c}{2}} (\sigma_{xc}\delta\varepsilon_{xc} + \sigma_{zc}\delta\varepsilon_{zc} + \tau_c\delta\gamma_c)dz \Bigg) dx\end{aligned} \tag{7}$$

2.2. Finite element formulation

2.2.1 Sandwich beam

A schematic of a representative sandwich beam element is illustrated in Fig. 1. Twenty degrees of freedom are allocated to six positions through the thickness in order to uniquely describe the displacement and strain fields in each layer through the thickness. In this respect, the nodal displacement vector corresponding to the i^{th} node is defined as:

$$\begin{aligned}\boldsymbol{u}_{(i)} = \big[&u_{tt(i)}\ u_{tb(i)}\ w_{t(i)}\ w_{t,x(i)} \\ &u_{ct(i)}\ u_{ct,x(i)}\ u_{ct,z(i)}\ u_{cb(i)}\ u_{cb,x(i)}\ u_{cb,z(i)}\ w_{ct(i)}\ w_{ct,x(i)}\ w_{ct,z(i)}\ w_{cb(i)}\ w_{cb,x(i)}\ w_{cb,z(i)} \\ &u_{bt(i)}\ u_{bb(i)}\ w_{b(i)}\ w_{b,x(i)}\big]^T\end{aligned} \tag{8}$$

$$\boldsymbol{u_e} = \begin{bmatrix}\boldsymbol{u}_{(i)} \\ \boldsymbol{u}_{(i+1)}\end{bmatrix} \tag{9}$$

where $\boldsymbol{u_e}$ is a generalized displacement vector.

According to Eqs. (8) and (9), the displacement functions at each layer can be expressed by multiplying of a shape function matrix in a displacement vector as:

$$u_j = \boldsymbol{N_j u_e} \quad w_j = \boldsymbol{M_j u_e} \qquad (j = t, b, c) \tag{10}$$

where $\boldsymbol{N}$ and $\boldsymbol{M}$ are matrices of shape functions describing the distribution of displacement through each layer of the sandwich element. According to the displacement field, the finite element formulation should be developed properly based on both Lagrange linear and Hermite cubic interpolation [31]. As shown in Fig. 2, shape functions are defined in local coordinates η, ξ $(-1 \le \eta, \xi \le 1)$ by:

$$\text{Linear: } \begin{cases} L_{(i)} = \frac{1}{2}(1-\eta) \\ L_{(i+1)} = \frac{1}{2}(1+\eta) \end{cases} \qquad \text{Hermite: } \begin{cases} H_{(i)} = \frac{1}{4}(\eta^3 - 3\eta + 2) \\ \bar{H}_{(i)} = \frac{l}{8}(\eta^3 - \eta^2 - \eta + 1) \\ H_{(i+1)} = \frac{1}{4}(-\eta^3 + 3\eta + 2) \\ \bar{H}_{(i+1)} = \frac{l}{8}(\eta^3 + \eta^2 - \eta - 1) \end{cases} \tag{11a}$$

$$\text{Linear: } \begin{cases} L_t = \frac{1}{2}(1+\xi) \\ L_b = \frac{1}{2}(1-\xi) \end{cases} \qquad \text{Hermite: } \begin{cases} H_b = \frac{1}{4}(\eta^3 - 3\eta + 2) \\ \bar{H}_b = \frac{h}{8}(\eta^3 - \eta^2 - \eta + 1) \\ H_t = \frac{1}{4}(-\eta^3 + 3\eta + 2) \\ \bar{H}_t = \frac{h}{8}(\eta^3 + \eta^2 - \eta - 1) \end{cases} \tag{11b}$$

where

$$\begin{cases} \eta = \dfrac{2(x - x_{(i)})}{l} - 1 \\ \xi = \dfrac{2(z - z_o)}{h} - 1 \end{cases} \tag{12}$$

The linear shape functions interpolate axial displacement in the face sheets while the Hermite shape functions are used for the vertical displacement to overcome shear locking phenomenon. The axial and vertical displacements in the core are approximated by using Hermite shape functions along both directions of x and z as:

$$\boldsymbol{N_t} = \left[L_{(i)}[L_t \;\; L_b] \;\; [0]_{1\times 18} \;\; L_{(i+1)}[L_t \;\; L_b] \;\; [0]_{1\times 18}\right] \tag{13a}$$

$$\boldsymbol{M_t} = \left[0 \;\; 0 \;\; \left[H_{(i)} \;\; \bar{H}_{(i)}\right] \;\; [0]_{1\times 18} \;\; \left[H_{(i+1)} \;\; \bar{H}_{(i+1)}\right] \;\; [0]_{1\times 16}\right] \tag{13b}$$

$$\boldsymbol{N_b} = \left[[0]_{1\times 16} \;\; L_{(i)}[L_t \;\; L_b] \;\; [0]_{1\times 18} \;\; L_{(i+1)}[L_t \;\; L_b] \;\; 0 \;\; 0\right] \tag{13c}$$

$$\boldsymbol{M_b} = \left[[0]_{1\times 18} \;\; \left[H_{(i)} \;\; \bar{H}_{(i)}\right] \;\; [0]_{1\times 18} \;\; \left[H_{(i+1)} \;\; \bar{H}_{(i+1)}\right]\right] \tag{13d}$$

$$\begin{aligned} \boldsymbol{N_c} = \big[[0]_{1\times 4} \;\; \left[H_{(i)}H_t \;\; \bar{H}_{(i)}H_t \;\; H_{(i)}\bar{H}_t\right] \;\; \left[H_{(i)}H_b \;\; \bar{H}_{(i)}H_b \;\; H_{(i)}\bar{H}_b\right] \\ [0]_{1\times 14} \left[H_{(i+1)}H_t \;\; \bar{H}_{(i+1)}H_t \;\; H_{(i+1)}\bar{H}_t\right] \;\; \left[H_{(i+1)}H_b \;\; \bar{H}_{(i+1)}H_b \;\; H_{(i+1)}\bar{H}_b\right] \;\; [0]_{1\times 10}\big] \end{aligned} \tag{13e}$$

$$\begin{aligned} \boldsymbol{M_c} = \big[[0]_{1\times 10} \;\; \left[H_{(i)}H_t \;\; \bar{H}_{(i)}H_t \;\; H_{(i)}\bar{H}_t\right] \;\; \left[H_{(i)}H_b \;\; \bar{H}_{(i)}H_b \;\; H_{(i)}\bar{H}_b\right] \\ [0]_{1\times 14} \left[H_{(i+1)}H_t \;\; \bar{H}_{(i+1)}H_t \;\; H_{(i+1)}\bar{H}_t\right] \;\; \left[H_{(i+1)}H_b \;\; \bar{H}_{(i+1)}H_b \;\; H_{(i+1)}\bar{H}_b\right] \;\; [0]_{1\times 4}\big] \end{aligned} \tag{13f}$$

where $\boldsymbol{N}$ and $\boldsymbol{M}$ are function of ξ and η in the local coordinate system as shown in Fig 2. Using Eq. (11), the derivatives of these functions are defined as:

$$\boldsymbol{N_{j,x}} = \frac{l}{2}\boldsymbol{N_{j,\eta}} \qquad \boldsymbol{N_{j,z}} = \frac{h_j}{2}\boldsymbol{N_{j,\xi}} \tag{14a}$$

$$\boldsymbol{M_{j,x}} = \frac{l}{2}\boldsymbol{M_{j,\eta}} \qquad \boldsymbol{M_{j,z}} = \frac{h_j}{2}\boldsymbol{M_{j,\xi}} \qquad (j = t, b, c) \tag{14b}$$

by substituting the discretized displacement field (10) into Eq. (2), the strain field of the sandwich element and its variational form can be expressed in a discretized form as:

$$\boldsymbol{\epsilon}:\begin{cases}\text{Face sheet:}\begin{cases}\epsilon_{xj}(\eta,\xi,\boldsymbol{u_e}) = \boldsymbol{N_{j,x}u_e} + \frac{1}{2}\left(\boldsymbol{N_{j,x}u_e}\right)^2 + \frac{1}{2}\left(\boldsymbol{M_{j,x}u_e}\right)^2 \\ \gamma_j(\eta,\xi,\boldsymbol{u_e}) = \boldsymbol{N_{j,z}u_e} + \boldsymbol{M_{j,x}u_e} + \left(\boldsymbol{N_{j,x}u_e}\right)\left(\boldsymbol{N_{j,z}u_e}\right)\end{cases} \quad (j=t,b) \\ \text{core:}\begin{cases}\epsilon_{xc}(\eta,\xi,\boldsymbol{u_e}) = \boldsymbol{N_{c,x}u_e} + \frac{1}{2}\left(\boldsymbol{N_{c,x}u_e}\right)^2 + \frac{1}{2}\left(\boldsymbol{M_{c,x}u_e}\right)^2 \\ \epsilon_{zc}(\eta,\xi,\boldsymbol{u_e}) = \boldsymbol{M_{c,z}u_e} + \frac{1}{2}\left(\boldsymbol{N_{c,z}u_e}\right)^2 + \frac{1}{2}\left(\boldsymbol{M_{c,z}u_e}\right)^2 \\ \gamma_c(\eta,\xi,\boldsymbol{u_e}) = \boldsymbol{N_{c,z}u_e} + \boldsymbol{M_{c,x}u_e} + \left(\boldsymbol{N_{c,x}u_e}\right)\left(\boldsymbol{N_{c,z}u_e}\right) + \left(\boldsymbol{M_{c,x}u_e}\right)\left(\boldsymbol{M_{c,z}u_e}\right)\end{cases}\end{cases} \tag{15}$$

$$\delta\boldsymbol{\epsilon}:\begin{cases}\delta\epsilon_{xj} = \delta\boldsymbol{u_e^T}\,\bar{\boldsymbol{N}}_{\boldsymbol{j}}^{\boldsymbol{T}}(\eta,\xi,\boldsymbol{u_e}) \\ \delta\epsilon_{zc} = \delta\boldsymbol{u_e^T}\,\hat{\boldsymbol{N}}_{\boldsymbol{c}}^{\boldsymbol{T}}(\eta,\xi,\boldsymbol{u_e}) \quad (j=t,c,b) \\ \delta\gamma_j = \delta\boldsymbol{u_e^T}\,\tilde{\boldsymbol{N}}_{\boldsymbol{j}}^{\boldsymbol{T}}(\eta,\xi,\boldsymbol{u_e})\end{cases} \tag{16}$$

where

$$\begin{cases}\text{Face sheet:}\begin{cases}\bar{\boldsymbol{N}}_{\boldsymbol{j}} = \boldsymbol{N_{j,x}}\left(1+\boldsymbol{N_{j,x}u_e}\right) + \boldsymbol{M_{j,x}}\left(\boldsymbol{M_{j,x}u_e}\right) \\ \tilde{\boldsymbol{N}}_{\boldsymbol{j}} = \boldsymbol{N_{j,z}}\left(1+\boldsymbol{N_{j,x}u_e}\right) + \boldsymbol{M_{j,x}} + \boldsymbol{N_{j,x}}\left(\boldsymbol{N_{j,z}u_e}\right)\end{cases} \quad (j=t,b) \\ \text{core:}\begin{cases}\bar{\boldsymbol{N}}_{\boldsymbol{c}} = \boldsymbol{N_{c,x}}\left(1+\boldsymbol{N_{c,x}u_e}\right) + \boldsymbol{M_{c,x}}\left(\boldsymbol{M_{c,x}u_e}\right) \\ \hat{\boldsymbol{N}}_{\boldsymbol{c}} = \boldsymbol{M_{c,z}}\left(1+\boldsymbol{M_{c,z}u_e}\right) + \boldsymbol{N_{c,z}}\left(\boldsymbol{N_{c,z}u_e}\right) \\ \tilde{\boldsymbol{N}}_{\boldsymbol{c}} = \boldsymbol{N_{c,z}}\left(1+\boldsymbol{N_{c,x}u_e}\right) + \boldsymbol{M_{c,x}}\left(1+\boldsymbol{M_{c,z}u_e}\right) + \boldsymbol{N_{c,x}}\left(\boldsymbol{N_{c,z}u_e}\right) + \boldsymbol{M_{c,z}}\left(\boldsymbol{M_{c,x}u_e}\right)\end{cases}\end{cases} \tag{17}$$

Next, by substituting Eqs. (15) and (16) into the stress field (3) and the subsequent result into the virtual strain energy (7), governing equations of the sandwich beam element are derived as:

$$\boldsymbol{f_{int}}(\boldsymbol{u_e}) - \boldsymbol{f_{ext}} = \boldsymbol{0} \tag{18}$$

in which

$$\boldsymbol{f_{int}} = \frac{bl}{4}\int_{-1}^{1}\int_{-1}^{1}\Big(h_t\left(\bar{\boldsymbol{N}}_{\boldsymbol{t}}^{\boldsymbol{T}}E_{xt}\epsilon_{xt} + \tilde{\boldsymbol{N}}_{\boldsymbol{t}}^{\boldsymbol{T}}G_{zxt}\gamma_t\right) + h_b\left(\bar{\boldsymbol{N}}_{\boldsymbol{b}}^{\boldsymbol{T}}E_{xb}\epsilon_{xb} + \tilde{\boldsymbol{N}}_{\boldsymbol{b}}^{\boldsymbol{T}}G_{zxb}\gamma_b\right) + h_c\left(\bar{\boldsymbol{N}}_{\boldsymbol{c}}^{\boldsymbol{T}}(Q_{xc}\epsilon_{xc} + Q_c\epsilon_{zc}) + \hat{\boldsymbol{N}}_{\boldsymbol{c}}^{\boldsymbol{T}}(Q_{zc}\epsilon_{zc} + Q_c\epsilon_{xc}) + \tilde{\boldsymbol{N}}_{\boldsymbol{c}}^{\boldsymbol{T}}G_{zxc}\gamma_c\right)\Big)\,d\xi\,d\eta \tag{19}$$

$$\boldsymbol{f_{ext}} = \begin{bmatrix}\boldsymbol{f}_{(i)} \\ \boldsymbol{f}_{(i+1)}\end{bmatrix} \tag{20}$$

where $\boldsymbol{f}_{(i)}$ is the mechanical load vector applied on the i^{th} node which can be expressed as:

$$\boldsymbol{f}_{(i)} = \left[P_{tt(i)}\;\; P_{tb(i)}\;\; V_{t(i)}\;\; 0\;\; P_{ct(i)}\;\; 0\;\; 0\;\; P_{cb(i)}\;\; 0\;\; 0\;\; V_{ct(i)}\;\; 0\;\; 0\;\; V_{cb(i)}\;\; 0\;\; 0\;\; P_{bt(i)}\;\; P_{bb(i)}\;\; V_{b(i)}\;\; 0\right]^T \tag{21}$$

in which P and V are generalized concentrated axial and transverse forces, respectively. The global FE governing equations of equilibrium for a sandwich beam can be obtained by using Eq. (21), assembling scheme and imposing boundary conditions. The final format of the equilibrium equations can be expressed as:

$$\boldsymbol{R} = \boldsymbol{F_{int}}(\boldsymbol{u}) - \boldsymbol{F_{ext}} \tag{22}$$

where $\boldsymbol{R}$ denotes the global residual vector. Eq. (22) is a highly non-linear algebraic equation in terms of nodal displacement vector. In order to solve the present problem with geometric and boundary-condition non-linearities, an iterative Newton–Raphson method [31] is implemented resulting in nodal displacements values. In this respect, a tangent matrix is defined as:

$$\boldsymbol{T} = \frac{\partial \boldsymbol{R}}{\partial \boldsymbol{u}} \tag{23}$$

and it can be expressed for each element as:

$$\begin{aligned}\boldsymbol{T_e} = \frac{bl}{4}\int_{-1}^{1}\int_{-1}^{1}\Big(&h_t\big(\bar{\boldsymbol{N}}_{\boldsymbol{t}}^{T}E_{xt}\bar{\boldsymbol{N}}_{\boldsymbol{t}} + \tilde{\boldsymbol{N}}_{\boldsymbol{t}}^{T}G_{zxt}\tilde{\boldsymbol{N}}_{\boldsymbol{t}}\big) + h_b\big(\bar{\boldsymbol{N}}_{\boldsymbol{b}}^{T}E_{xb}\bar{\boldsymbol{N}}_{\boldsymbol{b}} + \tilde{\boldsymbol{N}}_{\boldsymbol{b}}^{T}G_{zxb}\gamma_b\tilde{\boldsymbol{N}}_{\boldsymbol{b}}\big)\\ &+ h_c\big(\bar{\boldsymbol{N}}_{\boldsymbol{c}}^{T}\big(Q_{xc}\bar{\boldsymbol{N}}_{\boldsymbol{c}} + Q_c\hat{\boldsymbol{N}}_{\boldsymbol{c}}\big) + \hat{\boldsymbol{N}}_{\boldsymbol{c}}^{T}\big(Q_{zc}\hat{\boldsymbol{N}}_{\boldsymbol{c}} + Q_c\bar{\boldsymbol{N}}_{\boldsymbol{c}}\big) + \tilde{\boldsymbol{N}}_{\boldsymbol{c}}^{T}G_{zxc}\tilde{\boldsymbol{N}}_{\boldsymbol{c}}\big)\Big)d\xi d\eta\\ +\frac{bl}{4}\int_{-1}^{1}\int_{-1}^{1}\Big(&h_t\left(\acute{\bar{\boldsymbol{N}}}_{\boldsymbol{t}}E_{xt}\epsilon_{xt} + \acute{\tilde{\boldsymbol{N}}}_{\boldsymbol{t}}G_{zxt}\gamma_t\right) + h_b\left(\acute{\bar{\boldsymbol{N}}}_{\boldsymbol{b}}E_{xb}\epsilon_{xb} + \acute{\tilde{\boldsymbol{N}}}_{\boldsymbol{b}}G_{zxb}\gamma_b\right)\\ &+ h_c\left(\acute{\bar{\boldsymbol{N}}}_{\boldsymbol{c}}(Q_{xc}\epsilon_{xc} + Q_c\epsilon_{zc}) + \acute{\hat{\boldsymbol{N}}}_{\boldsymbol{c}}(Q_{zc}\epsilon_{zc} + Q_c\epsilon_{xc}) + \acute{\tilde{\boldsymbol{N}}}_{\boldsymbol{c}}G_{zxc}\gamma_c\right)\Big)d\xi d\eta\end{aligned} \tag{24}$$

in which

$$\begin{cases}\text{Face sheet:}\begin{cases}\acute{\bar{\boldsymbol{N}}}_{\boldsymbol{J}} = \bar{\boldsymbol{N}}_{\boldsymbol{j},\boldsymbol{u_e}} = \boldsymbol{N}_{\boldsymbol{j},x}^{T}\boldsymbol{N}_{\boldsymbol{j},x} + \boldsymbol{M}_{\boldsymbol{j},x}^{T}\boldsymbol{M}_{\boldsymbol{j},x}\\ \acute{\tilde{\boldsymbol{N}}}_{\boldsymbol{J}} = \tilde{\boldsymbol{N}}_{\boldsymbol{j},\boldsymbol{u_e}} = \boldsymbol{N}_{\boldsymbol{j},z}^{T}\boldsymbol{N}_{\boldsymbol{j},x} + \boldsymbol{N}_{\boldsymbol{j},x}^{T}\boldsymbol{N}_{\boldsymbol{j},z}\end{cases} \quad (j = t, b)\\ \text{core:}\begin{cases}\acute{\bar{\boldsymbol{N}}}_{\boldsymbol{c}} = \bar{\boldsymbol{N}}_{\boldsymbol{c},\boldsymbol{u_e}} = \boldsymbol{N}_{\boldsymbol{c},x}^{T}\boldsymbol{N}_{\boldsymbol{c},x} + \boldsymbol{M}_{\boldsymbol{c},x}^{T}\boldsymbol{M}_{\boldsymbol{c},x}\\ \acute{\hat{\boldsymbol{N}}}_{\boldsymbol{c}} = \hat{\boldsymbol{N}}_{\boldsymbol{c},\boldsymbol{u_e}} = \boldsymbol{M}_{\boldsymbol{c},z}^{T}\boldsymbol{M}_{\boldsymbol{c},z} + \boldsymbol{N}_{\boldsymbol{c},z}^{T}\boldsymbol{N}_{\boldsymbol{c},z}\\ \acute{\tilde{\boldsymbol{N}}}_{\boldsymbol{c}} = \tilde{\boldsymbol{N}}_{\boldsymbol{c},\boldsymbol{u_e}} = \boldsymbol{N}_{\boldsymbol{c},z}^{T}\boldsymbol{N}_{\boldsymbol{c},x} + \boldsymbol{N}_{\boldsymbol{c},x}^{T}\boldsymbol{N}_{\boldsymbol{c},z} + \boldsymbol{M}_{\boldsymbol{c},z}^{T}\boldsymbol{M}_{\boldsymbol{c},x} + \boldsymbol{M}_{\boldsymbol{c},x}^{T}\boldsymbol{M}_{\boldsymbol{c},z}\end{cases}\end{cases} \tag{25}$$

2.2.2 Fully 2D plane stress

For a fully 2D study, general displacement functions (u, w) are considered in the global XZ coordinate system. The Green strain tensor and the corresponding second Piola-Kirchhoff stress function can be derived for an orthotropic linear elastic material as:

$$\boldsymbol{\epsilon}:\begin{cases}\epsilon_x = u_{,x} + \frac{1}{2}(u_{,x}^{2} + w_{,x}^{2})\\ \epsilon_z = w_{,z} + \frac{1}{2}(u_{,z}^{2} + w_{,z}^{2})\\ \gamma = u_{,z} + w_{,x} + u_{,x}\,u_{,z} + w_{,x}\,w_{,z}\end{cases} \tag{26a}$$

$$\boldsymbol{\sigma}:\begin{cases}\sigma_x = Q_x\varepsilon_x + Q\varepsilon_z\\ \sigma_z = Q_z\varepsilon_{zc} + Q\varepsilon_x\\ \tau = G_{zx}\gamma\end{cases} \tag{26b}$$

where

$$Q_x = \frac{E_x}{(1-\frac{E_x}{E_z}\upsilon_{zx}^2)}, Q_z = \frac{E_z}{(1-\frac{E_x}{E_z}\upsilon_{zx}^2)}, Q = \frac{E_x\upsilon_{zx}}{(1-\frac{E_x}{E_z}\upsilon_{zx}^2)} \tag{27}$$

As shown in Fig 2b, a fully 2D FE model is stablished based on the quadratic element. In this respect, the displacement functions can be expressed by multiplying of a shape function matrix in a displacement vector as [31]:

$$u = \boldsymbol{N}\boldsymbol{u_e} \quad w = \boldsymbol{M}\boldsymbol{u_e} \tag{28}$$

in which

$$\boldsymbol{u_e} = \left[u_{(1)}\ w_{(1)}\ u_{(2)}\ w_{(2)}\ u_{(3)}\ w_{(3)}\ u_{(4)}\ w_{(4)}\ u_{(5)}\ w_{(5)}\ u_{(6)}\ w_{(6)}\ u_{(7)}\ w_{(7)}\ u_{(8)}\ w_{(8)}\right]^T \tag{29}$$

$$\boldsymbol{N}(\eta,\xi) = \left[N_{(1)}\ 0\ N_{(2)}\ 0\ N_{(3)}\ 0\ N_{(4)}\ 0\ N_{(5)}\ 0\ N_{(6)}\ 0\ N_{(7)}\ 0\ N_{(8)}\ 0\right] \tag{30}$$

$$\boldsymbol{M}(\eta,\xi) = \left[0\ N_{(1)}\ 0\ N_{(2)}\ 0\ N_{(3)}\ 0\ N_{(4)}\ 0\ N_{(5)}\ 0\ N_{(6)}\ 0\ N_{(7)}\ 0\ N_{(8)}\right] \tag{31}$$

where $N_{(i)}$ $(i = 1{\sim}8)$ are the quadratic shape functions in local coordinates which can be found in [31] as detailed below:

$$\begin{cases} N_1 = \frac{1}{4}(\eta^2-\eta)(\xi^2-\xi) \\ N_3 = \frac{1}{4}(\eta^2+\eta)(\xi^2-\xi) \\ N_5 = \frac{1}{4}(\eta^2+\eta)(\xi^2+\xi) \\ N_7 = \frac{1}{4}(\eta^2-\eta)(\xi^2+\xi) \end{cases} \quad \begin{cases} N_1 = \frac{1}{2}(1-\eta^2)(\xi^2-\xi) \\ N_3 = \frac{1}{2}(\eta^2+\eta)(1-\xi^2) \\ N_5 = \frac{1}{2}(1-\eta^2)(\xi^2+\xi) \\ N_7 = \frac{1}{2}(\eta^2-\eta)(1-\xi^2) \end{cases} \tag{32}$$

where

$$\begin{cases} \eta = \dfrac{2(x-x_{(i)})}{l} - 1 \\ \xi = \dfrac{2(z-z_{(1)})}{h} - 1 \end{cases} \tag{33}$$

In a similar way, the strain and stress functions are also discretized and then substituted into the Hamiltonian principle. Therefore, the governing equations of equilibrium can be derived in a matrix form as:

$$\boldsymbol{f_{int}}(\boldsymbol{u_e}) - \boldsymbol{f_{ext}} = \boldsymbol{0} \tag{34}$$

where

$$\boldsymbol{f_{int}} = \frac{bhl}{4}\int_{-1}^{1}\int_{-1}^{1}\left(\bar{\boldsymbol{N}}^T(Q_x\epsilon_x + Q\epsilon_z) + \hat{\boldsymbol{N}}^T(Q_z\epsilon_z + Q\epsilon_x) + \tilde{\boldsymbol{N}}^T G_{zx}\gamma\right)d\xi d\eta \tag{35}$$

$$\boldsymbol{f_{ext}} = \left[P_{(1)}\ V_{(1)}\ P_{(2)}\ V_{(2)}\ P_{(3)}\ V_{(3)}\ P_{(4)}\ V_{(4)}\ P_{(5)}\ V_{(5)}\ P_{(6)}\ V_{(6)}\ P_{(7)}\ V_{(7)}\ P_{(8)}\ V_{(8)}\right]^T \tag{36}$$

$$\begin{cases} \bar{\boldsymbol{N}} = \boldsymbol{N}_{,x}\,(1+\boldsymbol{N}_{,x}\,\boldsymbol{u}_e) + \boldsymbol{M}_{,x}\,(\boldsymbol{M}_{,x}\,\boldsymbol{u}_e) \\ \hat{\boldsymbol{N}} = \boldsymbol{M}_{,z}\,(1+\boldsymbol{M}_{,z}\,\boldsymbol{u}_e) + \boldsymbol{N}_{,z}\,(\boldsymbol{N}_{,z}\,\boldsymbol{u}_e) \\ \tilde{\boldsymbol{N}} = \boldsymbol{N}_{,z}\,(1+\boldsymbol{N}_{,x}\,\boldsymbol{u}_e) + \boldsymbol{M}_{,x}\,(1+\boldsymbol{M}_{,z}\,\boldsymbol{u}_e) + \boldsymbol{N}_{,x}\,(\boldsymbol{N}_{,z}\,\boldsymbol{u}_e) + \boldsymbol{M}_{,z}\,(\boldsymbol{M}_{,x}\,\boldsymbol{u}_e) \end{cases} \tag{37}$$

In order to implement the Newton-Raphson method, the tangent matrix should be determined for each element as:

$$\boldsymbol{T}_e = \frac{\partial \boldsymbol{f}_{int}}{\partial \boldsymbol{u}_e} \tag{38}$$

where

$$\begin{aligned} \boldsymbol{T}_e = \frac{bhl}{4}\int_{-1}^{1}\int_{-1}^{1}\left(\bar{\boldsymbol{N}}^T\left(Q_x\bar{\boldsymbol{N}}+Q\hat{\boldsymbol{N}}\right)+\hat{\boldsymbol{N}}^T\left(Q_z\hat{\boldsymbol{N}}+Q\bar{\boldsymbol{N}}\right)+\tilde{\boldsymbol{N}}^T G_{zx}\tilde{\boldsymbol{N}}\right)d\xi d\eta \\ +\frac{bhl}{4}\int_{-1}^{1}\int_{-1}^{1}\left(\acute{\bar{\boldsymbol{N}}}(Q_x\epsilon_x+Q\epsilon_z)+\acute{\hat{\boldsymbol{N}}}(Q_z\epsilon_z+Q\epsilon_x)+\acute{\tilde{\boldsymbol{N}}}G_{zx}\gamma\right)d\xi d\eta \end{aligned} \tag{39}$$

$$\begin{cases} \acute{\bar{\boldsymbol{N}}} = \bar{\boldsymbol{N}}_{,\boldsymbol{u}_e} = \boldsymbol{N}_{,x}^T\,\boldsymbol{N}_{,x} + \boldsymbol{M}_{,x}^T\,\boldsymbol{M}_{,x} \\ \acute{\hat{\boldsymbol{N}}} = \hat{\boldsymbol{N}}_{,\boldsymbol{u}_e} = \boldsymbol{M}_{,z}^T\,\boldsymbol{M}_{,z} + \boldsymbol{N}_{,z}^T\,\boldsymbol{N}_{,z} \\ \acute{\tilde{\boldsymbol{N}}} = \tilde{\boldsymbol{N}}_{,\boldsymbol{u}_e} = \boldsymbol{N}_{,x}^T\,\boldsymbol{N}_{,z} + \boldsymbol{N}_{,z}^T\,\boldsymbol{N}_{,x} + \boldsymbol{M}_{,x}^T\,\boldsymbol{M}_{,z} + \boldsymbol{M}_{,z}^T\,\boldsymbol{M}_{,x} \end{cases} \tag{40}$$

2.3. Interface condition

The interface between the face sheet and the core is an independent layer which should be described with extra conditions. As shown in Fig. 3, these conditions on the top interface are demonstrated for fully bonded and delaminated regions. For a fully bonded case, displacements of core at the top boundary are exactly followed by the top face sheet which results in normal and shear stresses at the interface surface. For a delaminated zone, the real contact conditions are enforced using the explicit algorithm of master-slave contact pair [31]. Nodes on the face sheets are considered as master nodes which can penetrate to the slave surface on top boundary of the core. However, the j^{th} node on the slave surface has always the closest distance to the i^{th} master node. As shown in Fig. 3, the local coordinate system (n, t) is defined by normal and tangential vectors on the interface at the contact point. For a frictionless contact, the master node can slide on the slave surface $(\tau_{it} = 0)$ while the movement is constrained along the normal direction by:

$$\begin{aligned} &\bar{w}_{tb(i)} \geq \bar{w}_{ct(j)} \quad \rightarrow \quad \sigma_{it(i)} = \sigma_{it(j)} \\ &\bar{w}_{tb(i)} < \bar{w}_{ct(j)} \quad \rightarrow \quad \sigma_{it(i)} = \sigma_{it(j)} = \lambda_{it}\bar{\bar{w}}_{it} \qquad \bar{\bar{w}}_{it} = \left(\bar{w}_{tb(i)} - \bar{w}_{ct(j)}\right) \end{aligned} \tag{41}$$

where σ_{it}, τ_{it}, $\bar{\bar{w}}_{it}$ and λ_{it} indicate the normal stress, shear stress, penetration and the Lagrange multiplier at the top interface surfaces, respectively. $\bar{w}$ is also the movement along the normal direction defined as:

$$\bar{w}_{tb(i)} = -\left(x_{(i)} + u_{tb(i)}\right)\sin\beta + w_{t(i)}\cos\beta \tag{42}$$

$$\bar{w}_{ct(j)} = -\left(x_{(j)} + u_{ct(j)}\right)\sin\beta + w_{ct(j)}\cos\beta$$

Eq. (41) includes appending of variations of Lagrange multiplier term in the global equilibrium equations for each contact slave and master nodes. In a similar way, the extra conditions describe the behaviors of interface between bottom face sheet and the core.

The solving process is started by predicting a configuration without considering the contact conditions. The penetration values of master nodes can then be calculated according to the predicted configuration. The global governing equilibrium equations will be updated based on new contact conditions at the delaminated regions. The iterative algorithm will be repeated until global displacement vector converges to a unique answer.

3. Numerical results and discussion

In order to verify and validate the presented FE models for the nonlinear analysis of sandwich beams with partially delaminated areas, the predictions of models are compared with relevant results in the open literature. After validation, some examples are studied to examine effects of boundary condition, number and position of delaminated regions on the response of sandwich beams.

For the first validation study, a sandwich beam as shown in Fig. 4a consisting of two face sheets made of Kevlar and a lightweight, low strength core of Rohacell with the following properties is analyzed.

$$\begin{aligned} &L = 300mm, \quad E_{xt} = E_{xb} = 27.42GPa, \\ &b = 60mm, \quad E_{zc} = 52.5MPa, \quad G_{zxc} = 21MPa \end{aligned} \tag{43}$$

Figs. 4b-4d display numerical results in terms of load versus mid-span top displacement, vertical displacements in face sheets along half-length of the beam, interfacial vertical normal stress at core-face interface and shear stress in core, respectively. They are obtained from the present 2D model and sandwich model and compared with those from analytical solution and FE solution obtained with ADINA, ver. 8.1 and ANSYS ver. 7.1 [16]. The analytical solution [16] assumed zero axial stress for the core and von-Karman strains for the face sheets. ADINA and ANSYS [16] assumed green strains for the core and face sheets. Fig. 4b shows that the results of all models are almost identical in the linear regime. In the large displacement range, the simplified analytical model [16] reveals that the displacement increases with the increase of the load, while other models predict an increasing-decreasing trend in the force. It is also observed that the FE results of the present 2D model and sandwich model are close to those from ADINA and ANSYS to some extent verifying the accuracy of the developed models. ADINA and ANSYS assumed the ratio of 1/500 between the modulus of elasticity of the core to that of the face sheets producing numerical difficulties in these software packages. The low modulus of elasticity of the core causes

large distortions in the core elements, which are beyond the numerical capabilities of ordinary elements used in ADINA, ANSYS and present 2D FE model. In this respect, the sandwich model is more accurate than the others and shows a high robustness. It should be mentioned that 2D FE model is not able to track the equilibrium path due to singularity in stiffness or tangent matrices in the large displacement and rotation regime. Regarding the results presented in Fig. 4c and 4d, it is found that the sandwich beam model developed in this work can accurately simulate the bending deflection and stresses of the beam compared to those reported in Ref. [16]. In this regard, it is seen that the analytical solution [16] overestimates the deflection and stresses compared to 2D FE and sandwich models specially in the central region.

Next, the accuracy of the present model in investigating the influence of the debonded interface on the non-linear behaviors for a sandwich beam is examined and the results are compared with those reported in Ref. [18]. The sandwich beam is loaded under three-point bending where the upper face-core interface is delaminated, 20 and 40 *mm* long, and the load is applied either at the upper or at the lower face sheet, see Figs. 5a and 6a. The beam is simply supported at the edges of the lower face sheet and the edges of the upper face sheet and the core are stress free and free to move. The material properties of the sandwich are assumed as presented in Eq. (43). Two cases are investigated dealing with a long and short delamination at the upper face-core interface where the load is applied either at the upper delaminated face sheet or at the lower bonded face sheet, see Figs. 5a and 6a. Figs. 5b, 5c, 5d show the results in terms of load versus mid-span top displacement, vertical displacements in face sheets along half-length of the beam, interfacial vertical normal stress at core-face interfaces and shear stress in core for the first case as depicted in Fig. 5a. The counterpart of these figures for the second case as shown Fig. 6a is presented in Figs. 6b, 6c, 6d. Ref. [18] assumed the core to have zero axial and shear stresses and constant vertical stress in the delaminated regions and von-Karman strains for the face sheets.

The results presented in Fig. 5b reveal that the non-linear responses of the sandwich beam loaded at the upper delaminated face sheet from both sandwich beam and 2D beam models are very close in both linear and nonlinear regimes. It is seen that these models predict deflections far lower than the model developed in [18]. It shows that considering the stress in the core plays an important role on the response of the sandwich beams and it cannot be ignored. By focusing on Fig. 6b, it can be found that there is a slight difference between responses from the sandwich beam and 2D beam models in linear and nonlinear ranges when the load is applied at the lower bonded face sheet. In this case, the sandwich beam model mostly predicts a lower deflection for any force. By comparing the results from the models developed in this research and Frostig and Thomsen's model [18], it is observed that the predictions are very different revealing the accuracy of the present models and assumptions. Fig. 5c reveals how the deformation pattern of the delaminated face sheet changes meaningfully along the length. In the region far from the delaminated part, two faces nearly move together with some small indentation displacements and with very small contact stresses, see Figs. 5c and 5d. In the delaminated region, the upper face sheet buckles upwards, but remains partially in contact with the upper face of the core. The core shear stresses display the

same trends as can be seen in Fig. 5d. These stresses are extremely high at the edges of the delaminated interface. Fig. 5d also reveals that the normal stresses at the upper and lower face-core interfaces are greatly high at the right tip of the delamination zone. Stresses change from compression to tension in the upper interface between the left and right tips of the delaminated region. Regarding the sandwich beam with a smaller delamination zone and with mechanical loading on the lower face sheet, Figs. 6c and 6d show that the vertical displacement of the loaded lower face is greater than that of the upper face reflected by zero contact stresses in the delaminated region. The upper face sheet experiences the buckling phenomenon in the debonded region. The core shear and normal stresses as shown Fig. 6d appear to be uniform through a large section of the sandwich beam, except in the vicinities of the delamination zone. In the edges of the delaminated region, a large jump occurs and a change in the stress sign is seen.

Next, a cantilever sandwich beam with debonding interfaces at the clamped end is considered to investigate the effects of debonding location and moving of contact points by implementing the present sandwich beam model, see Fig. 7a. At the clamped edge, all displacements and rotations are fully constrained in face sheets while they are free in the core. Mechanical response of fully bonded sandwich beam (C1) under tip-point load is compared with results of sandwich beams with debonding regions at top interface (C2), at bottom interface (C3) and at both interfaces (C4). Figs. 7b-7d show the results in terms of load versus tip displacement, interfacial normal stress at core-upper face interfaces and shear stress in core, respectively. The final configuration and distribution of core von-Mises stress of the sandwich beam at the end of loading are also shown in Figs. 8a-8d for C1-C4, respectively. As seen in Fig. 7b, both the location of delamination and direction of loading have significant effects on the beam stiffness (difference is almost 6 times more for local buckling force) even in the small deformation regime. Figs. 7c and 7d also show that sandwich beams C1 and C2 experience extreme stresses specially in the first half of the structure in the delamination area. The local buckling that happens at the clamped edge is the main reason of reduction of structural stiffness in all cases, see Figs. 8a-8d. The buckling mode in sandwich beams of C2, C3 and C4 with delaminated interfaces is different from the one happening in the fully bonded case of C1. Even though the buckling mode is similar in delaminated interfaces, the response of case C2 is far different from the other cases. The main reason of this difference is the effect of core at the delaminated region. It reveals the fact that the stress in the delaminated part of the core is significant and can not be neglected in contrary to Ref. [18]. As can be seen in Figs. 8b, 8c and 8d, unlike cases C3 and C4, the distribution of stress is highlighted at the bottom interface of delaminated section in case C2 while there is no contact at the delaminated top interface. In other words, it indicates that there are normal and shear stresses at bonded interfaces while there is no contact at the delaminated interface and it extremely affects the structural stiffness. Therefore, it is necessary to consider the stress distribution at each interface independently. On the other hand, both beam configurations and history of force-displacement paths for case C3 with delamination at bottom interface are so close to case C4 which has delamination on both interfaces. In both cases, the core does not have significant effects on the structural stiffness because of low level of stresses in the delaminated section, see Fig. 8.

The effects of quality of the bonding interfaces on the mechanical behavior of a sandwich beam under three-point bending is investigated. In this respect, a continuous bonding-delaminated pattern is considered for both top and bottom interfaces, see Fig. 9a. The responses of the sandwich beam for various delamination length, d, are presented in Fig. 9. Figs. 9b and 9c show the results in terms of load versus top-mid-span displacement and vertical displacement in top face sheet along half-length of the beam. The configuration and distribution of core von-Mises stress of the sandwich beam at the end of loading are also shown in Fig. 10-. As shown in Fig. 9b, the force-displacement path as well as local buckling point are affected by the delamination length specially in the large deformation range. It this respect, the longer the delamination length, the greater the deflection. The delamination length also affects the buckling phenomena. Figs. 9b, 9c, and 10a-10f reveal that the sandwich beam with delamination of $d = 40\ mm$ has a limit point at *F=400 N* when the first buckling occurs in the closest delamination zone to the middle of beam and then the structure experiences its second buckling at *F=800 N* in the delaminated zone next to the first buckled zone. The second buckling is seen as a drop in the force-deflection curve for the case of $d = 40\ mm$. However, it can be found that other cases have an increasing monotonic force-deflection curve that means all delaminated zones buckle together with different amplitudes. It should be mentioned that taking the stress in the delaminated zone core and stress distribution at each interface independently into the account is crucial to observe these new phenomena. It is also found that depending on the beam geometries and loading conditions, there is a critical length for delamination which can describe the quality of bonding at interfaces. For example, in this case, by considering local buckling mode and force history, the fully bonded conditions can be considered for interfaces with delamination less than $d = 10\ mm$. By increasing the length of delamination, the effects of core on the structural stiffness are decreased and consequently the local buckling happens at lower bending forces. As can be seen in Figs. 10c, 10d and 10f, the longer the delaminated zone, the larger the buckled face sheet.

4. Conclusion

The main objective of this paper was to introduce a new sandwich beam element for the analysis of sandwich structures with a flexible core and containing partially delaminated regions with high accuracy. The interfaces between the core and face sheets were modeled by two independent layers. The high-order sandwich panel theory was assumed to model the flexibility of the core with nonlinearities associated with geometric and real contact characteristics of the delaminated regions. The kinematics featured the continuity conditions for displacements and rotations at the interfaces for both fully bounded and delaminated regions. FE governing equations were developed based on the Hermite shape functions by implementing the Hamilton's principle and solved by using Newton-Raphson iterative approach. A 2D FE method was also stablished and the capability of the sandwich model was examined by a comparative study with 2D results. A good correlation was found between results from both sandwich and 2D FE models. It was found that they can predict large-deformation results for the sandwich behaviors much better than the

simplified model available in the literature. It was concluded that modeling the delaminated zone core and stress distribution at each interface independently is crucial to accurately analyze instability behaviors of sandwich structures. The implications of delamination features on the bending and local buckling response of sandwich beams were put into evidence via a parametric study, and pertinent conclusions were outlined. The following main results can be concluded:

1. Describing core displacements by interface displacement functions provides more robust stiffness/tangent matrices and removes singularity.

2. Considering independent displacement fields for each layer allows to apply different interface conditions.

3. Numerical results show non-zero distribution of the shear stress through the core with delamination where there is no contact.

4. Numerical results reveal the significant effects of length in continuous delaminations on the beam stiffness and local buckling shape modes.

Due to lack of any accurate sandwich model in the specialized literature, the developed model and the results supplied in the present work are expected to be instrumental toward a reliable design of sandwich beams with local delaminations.

References

[1] R.A. Di Taranto, Theory of vibratory bending for elastic and viscoelastic layered finite length beams, J. Appl. Mech. 87-88 (1965) 1-6.

[2] S.M.R. Khalili, A.R. Damanpack, N. Nemati, K. Malekzadeh, Free vibration analysis of sandwich beam carrying sprung masses, Int. J. Mech. Sci. 52 (2010) 1620-1633.

[3] Y. Frostig, Behavior of delaminated sandwich beam behavior with transversely flexible core – high order theory, Compos. Struct. 20 (1992) 1-16.

[4] M. Linke, W. Wohlers, H.G. Reimerdes, Finite Element for the Static and Stability Analysis of Sandwich Plates, J. Sandwich Struct. Mater. 9 (2007) 123–142.

[5] J.J.R.B. Bekuit, D.C.D. Oguamanam, O.A. Damisa, quasi finite element formulation for the analysis of sandwich beams, Fin. Elem. Anal. Des. 43 (2007) 1099–1107.

[6] C.N. Phan, N.W. Bailey, G.A. Kardomateas, Wrinkling of sandwich wide panels/beams based on the extended high-order sandwich panel theory: formulation,comparison with elasticity and experiments, Arch. Appl. Mech. 82 (2012) 1585–1599.

[7] C.N. Phan, G.A. Kardomateas, Y. Frostig, Global buckling of sandwich beams based on the extended high-order theory, AIAA J. 50 (2012) 1707–1716.

[8] Y. Frostig, C.N. Phan, G.A. Kardomateas, Free vibration of unidirectional sandwich panels, Part I: Compressible core, J. Sandwich Struct. Mater. 15 (2013) 377–411.

[9] D. Elmalich, O. Rabinovitch, A high-order finite element for dynamic analysis of soft-core sandwich plates, Int. J. Sandwich. Struct. Mater. 14 (2012) 525-555.

[10] D. Elmalich, O. Rabinovitch, Twist in soft-core sandwich plates, Int. J. Sandwich. Struct. Mater. 16 (2014) 577-613.

[11] M.M. Kheirikhah, S.M.R. Khalili, K. Malekzadeh Fard, Analytical solution for bending analysis of soft-core composite sandwich plates using improved high-order theory, Struct. Eng. Mech. 44 (2012) 15-34.

[12] A.R. Damanpack, M. Shakeri, M.M. Aghdam, A new finite element model for low-velocity impact analysis of sandwich beams subjected to multiple projectiles, Compos. Struct. 104 (2013) 21-33.

[13] A.R. Damanpack, M. Bodaghi, M.M. Aghdam, M. Shakeri, Active control of geometrically non-linear transient response of sandwich beams with a flexible core using piezoelectric patches, Compos. Struct. 100 (2013) 517-531.

[14] K. Magnucki, W. Szyc, M.J. Smyczynski, Strength and buckling of a sandwich beam with thin binding layers between faces and a metal foam core, Steel Compos. Struct. An Int'l J. 16 (2014) 325-337.

[15] Y. Frostig, V. Sokolinsky, Higher-order buckling of debonded (delaminated) sandwich panels with soft core, AIAA J. 38 (2000) 2147-2159.

[16] Y. Frostig, O.T. Thomsen, I. Sheinman, On the non-linear high-order theory of unidirectional sandwich panels with a transversely flexible core, Int. J. Solid. Struct. 42 (2005) 1443–1463.

[17] Y. Frostig, Geometrically nonlinear response of modern sandwich panels – distributed loads and localized effects, Int. J. Sandwich. Struct. Mater. 8 (2006) 539-556.

[18] Y. Frostig, O.T. Thomsen, Non-linear behavior of delaminated unidirectional sandwich panels with partial contact and a transversely flexible core, Int. J. Non-Linear Mech. 40 (2005) 633 – 651.

[19] H. Schwarts-Givli, O. Rabinovitch, Y. Frostig, High-order nonlinear contact effects in the dynamic behavior of delaminated sandwich panels with a flexible core, Int. J. Solid. Struct. 44 (2007) 77-99.

[20] Y.Frostig, O.T. Thomsen, Non-linear thermo-mechanical behavior of delaminated curved sandwich panels with a compliant core, Int. J. Solid. Struct. 48 (2011) 2218-2237.

[21] Y. Frostig, Non-linear behavior of a face-sheet debonded sandwich panel – Thermal effects, Int. J. Non-Linear Mech. 64 (2014) 1-25.

[22] W.B. Kim, B.J. Choi, Shear strength of connections between open and closed steel-concrete composite sandwich structures, Steel. Compos. Struct. An Int'l J. 11 (2011) 169-181.

[23] S.J. Hilo, W.W. Badaruzzaman, S.A. Osman, A.W. Al-Zand, M. Samir, Q.A. Hasan, A state-of-the-art review on double-skinned composite wall systems, Thin-Walled Structures, 97 (2015) 74-100.

[24] M.M. Shokrieh, M.Heidari-Rarani, A comparative study for beams on elastic foundation models to analysis of mode-I delamination in DCB specimens, Struct. Eng. Mech. An Int'l J. 37 (2011) 149-162.

[25] L. Liu, D.W. Shu, Free vibration analysis of rotating Timoshenko beams with multiple delaminations, Compos. Part B, 44 (2013) 733-739.

[26] M. Marjanovic, D. Vuksanovic, Layerwise solution of free vibrations and buckling of laminated composite and sandwich plates with embedded delaminations, Compos. Struct. 108 (2014) 9-20.

[27] M. McElroy, F. Leone, J. Ratcliffe, M. Czabaj, F.G. Yuan, Simulation of delamination–migration and core crushing in a CFRP sandwich structure, Compos. Part A. 79 (2015)192-202.

[28] R.M.J. Groh, A. Tessler, Computationally efficient beam elements for accurate stresses in sandwich laminates and laminated composites with delaminations, Comput. Methods Appl. Mech. Engrg. 320 (2017) 369–395.

[29] M. Pietrek, P. Horst, Analysis and numerical prediction of the delamination behavior of debonded asymmetric sandwich shells with a thin-walled skin considering plastic deformation, Compos. Struct. 188 (2018) 220–232.

[30] S. Kapuria, A. Ahmeda, An efficient zigzag theory based finite element modeling of composite and sandwich plates with multiple delaminations using a hybrid continuity method, Comput. Methods Appl. Mech. Engrg. 345 (2019) 212–232.

[31] O.C. Zienkiewicz, R.L. Taylor, The finite element method, McGrawHill, London, 1994.

Figure Captions

Fig. 1. Coordinate system and notations for a five-layer sandwich beam element.

Fig. 2. Local coordinate system for: (a) sandwich beam layers; (b) 2D plane stress.

Fig. 3. Top interface conditions: (a) fully bonded; (b) delaminated with contact; (c) delaminated without contact.

Fig. 4. Comparison between predictions of models for the sandwich beam under three-point bending: (a) geometry; (b) load versus mid-span displacement; (c) vertical displacements in face sheets along half-length of the beam; (d) interfacial vertical normal stress at core-face interfaces and shear stress in core.

Fig. 5. Comparison between predictions of models for the sandwich beam with an upper mid-span delamination under three-point bending: (a) geometry of the sandwich under a load applied at the upper delaminated face sheet; (b) load versus mid-span displacement; (c) vertical displacements in face sheets along half-length of the beam; (d) interfacial vertical normal stress at core-face interfaces and shear stress in core.

Fig. 6. Comparison between predictions of models for the sandwich beam with an upper mid-span delamination under three-point bending: (a) geometry of the sandwich under a load applied at the lower bonded face sheet; (b) load versus mid-span displacement; (c) vertical displacements in face sheets along half-length of the beam; (d) interfacial vertical normal stress at core-face interfaces and shear stress in core.

Fig. 7. Geometry and numerical results obtained for cantilever sandwich beams with upper or/and lower end delamination under the load applied on the upper face sheet at the tip point: (a) geometry; (b) load versus tip displacement; (c) interfacial axial normal stress at core-upper face interfaces and shear stress in core; (d) interfacial axial normal stress at core-lower face interfaces and shear stress in core.

Fig. 8. Final configuration and von-Mises stress distribution of the sandwich beam C1-C4 as depicted in Fig. 7a at the end of loading.

Fig. 9. Geometry and numerical results obtained for clamped sandwich beams with upper continuous delaminations under a point load applied on the upper face sheet at the mid span: (a) geometry; (b) load versus top-mid-span displacement; (c) vertical displacements in top face sheet along half-length of the beam for various values of d.

Fig. 10. Configuration and distribution of von-Misses stress of the core related to Fig. 9a for (d) $d = 0$; (e) $d = 10\ mm$; (f) $d = 16\ mm$; (g) $d = 20\ mm$; (h) $d = 30\ mm$; and (i) $d = 40\ mm$.

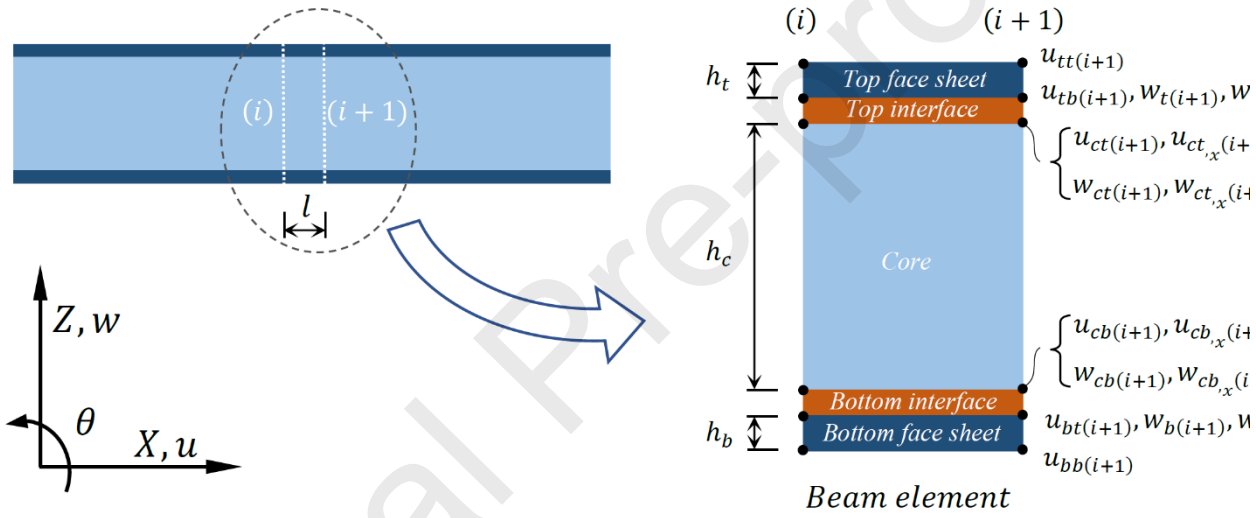

Fig. 1. Coordinate system and notations for a five-layer sandwich beam element.

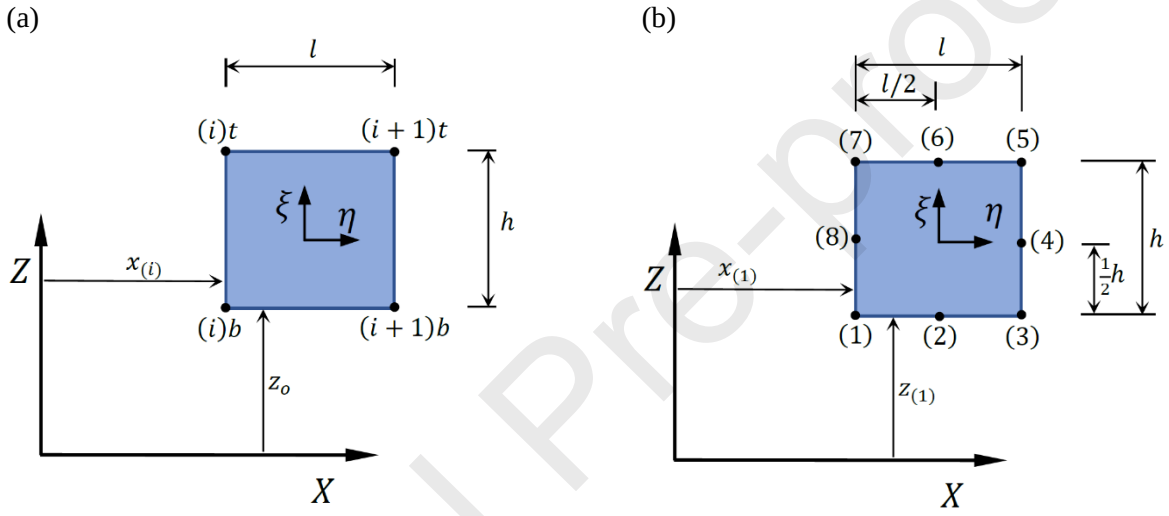

Fig. 2. Local coordinate system for: (a) sandwich beam layers; (b) 2D plane stress.

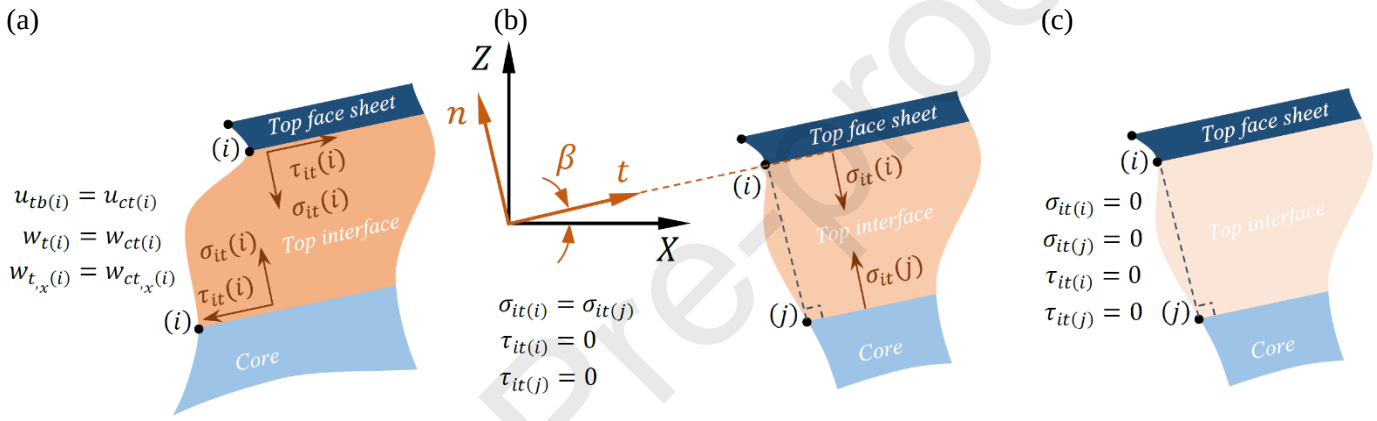

Fig. 3. Top interface conditions: (a) fully bonded; (b) delaminated with contact; (c) delaminated without contact.

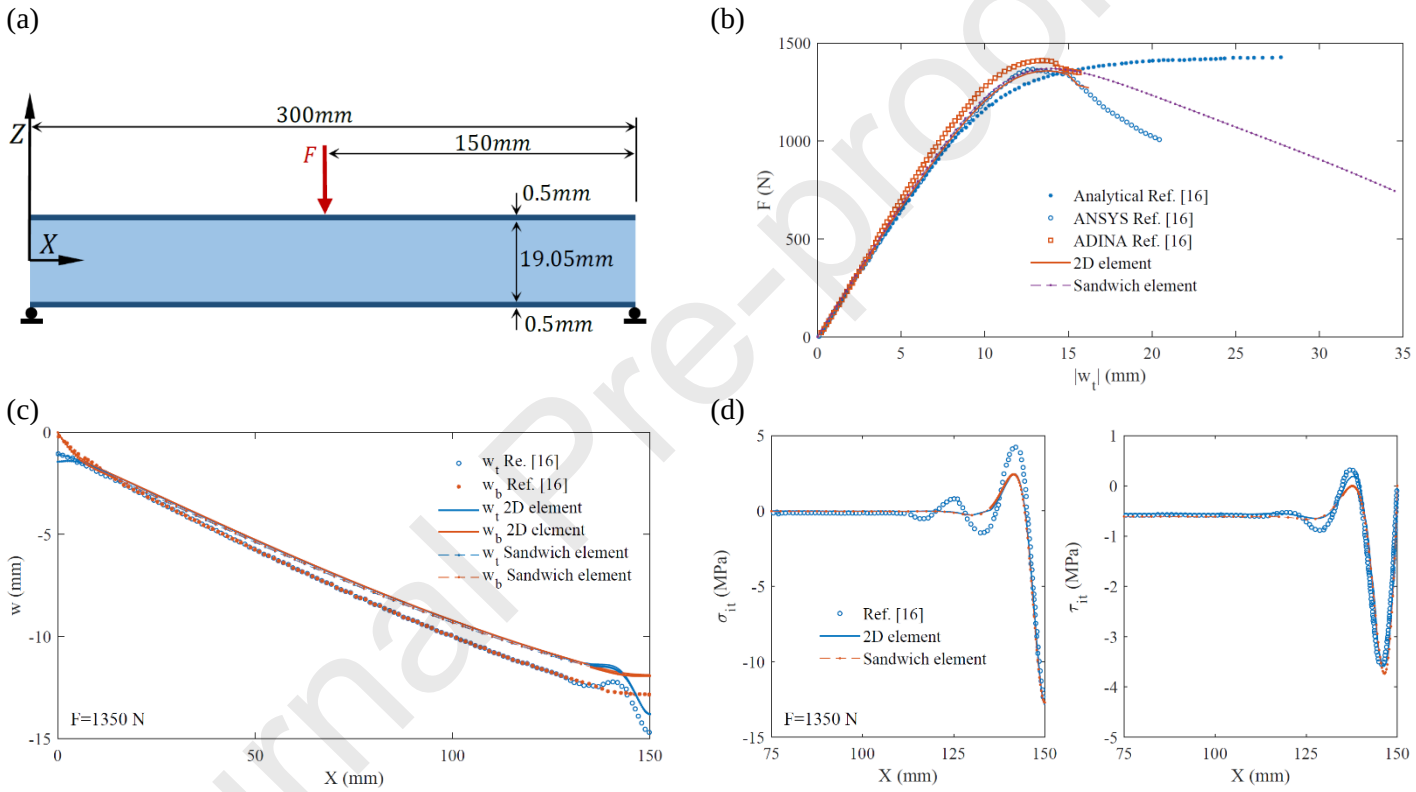

Fig. 4. Comparison between predictions of models for the sandwich beam under three-point bending: (a) geometry; (b) load versus mid-span displacement; (c) vertical displacements in face sheets along half-length of the beam; (d) interfacial vertical normal stress at core-face interfaces and shear stress in core.

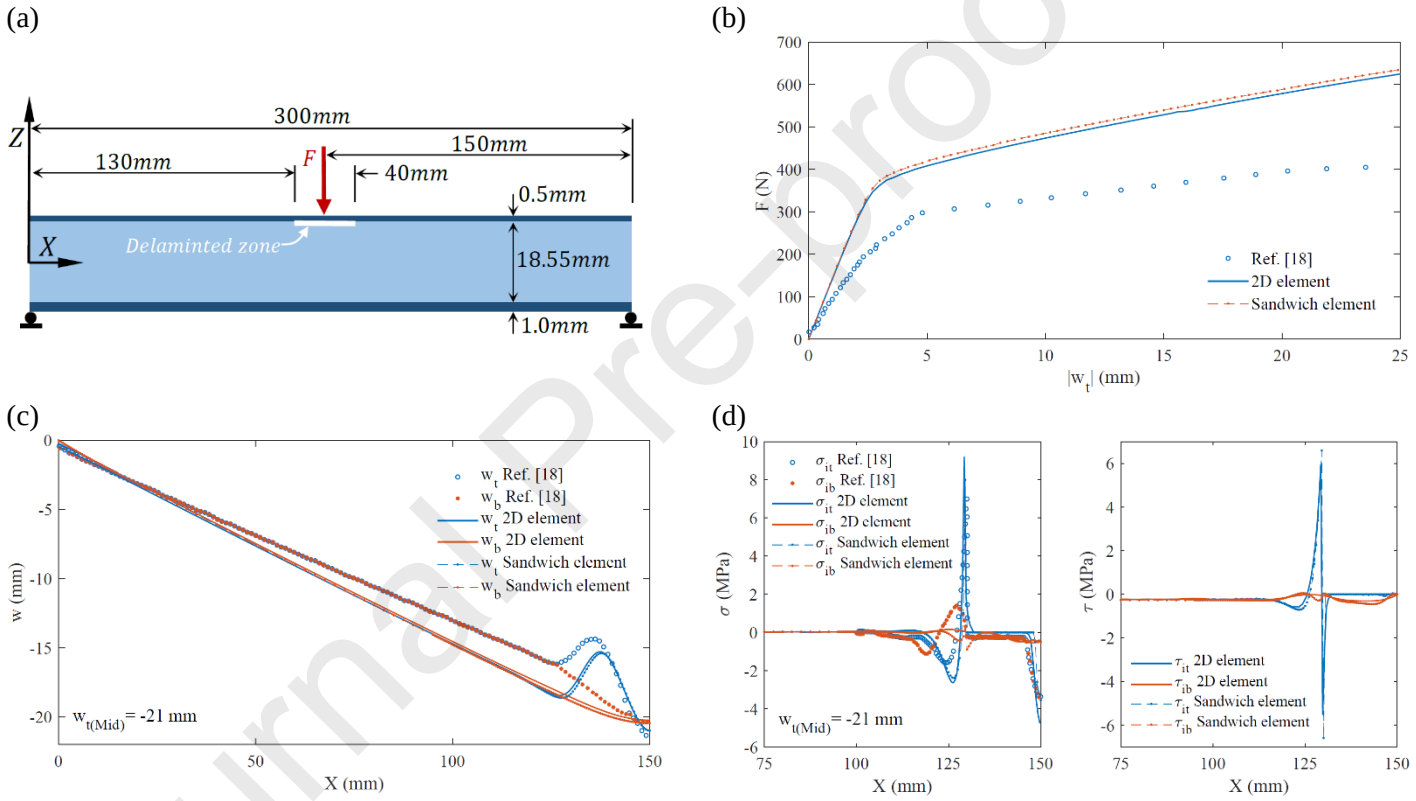

Fig. 5. Comparison between predictions of models for the sandwich beam with an upper mid-span delamination under three-point bending: (a) geometry of the sandwich under a load applied at the upper delaminated face sheet; (b) load versus mid-span displacement; (c) vertical displacements in face sheets along half-length of the beam; (d) interfacial vertical normal stress at core-face interfaces and shear stress in core.

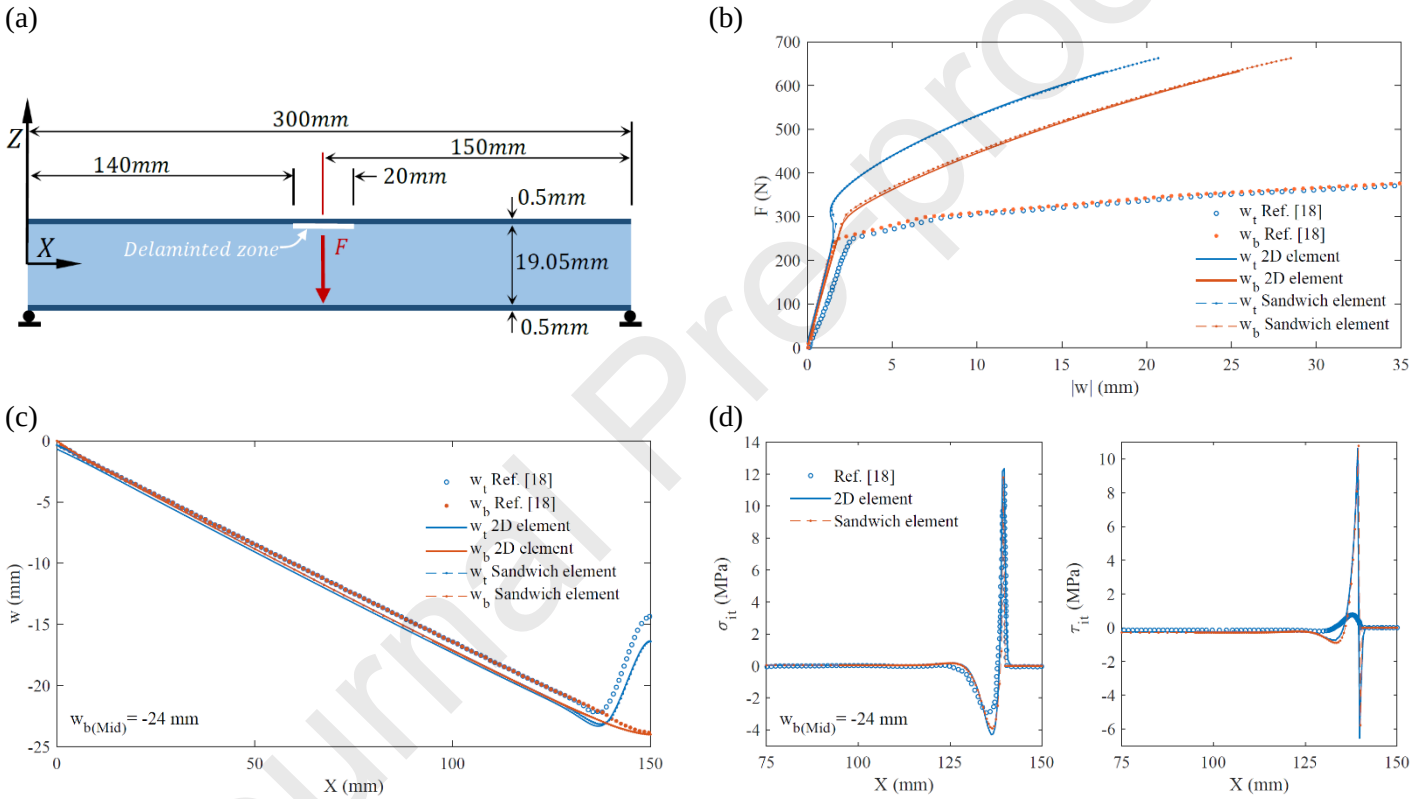

Fig. 6. Comparison between predictions of models for the sandwich beam with an upper mid-span delamination under three-point bending: (a) geometry of the sandwich under a load applied at the lower bonded face sheet; (b) load versus mid-span displacement; (c) vertical displacements in face sheets along half-length of the beam; (d) interfacial vertical normal stress at core-face interfaces and shear stress in core.

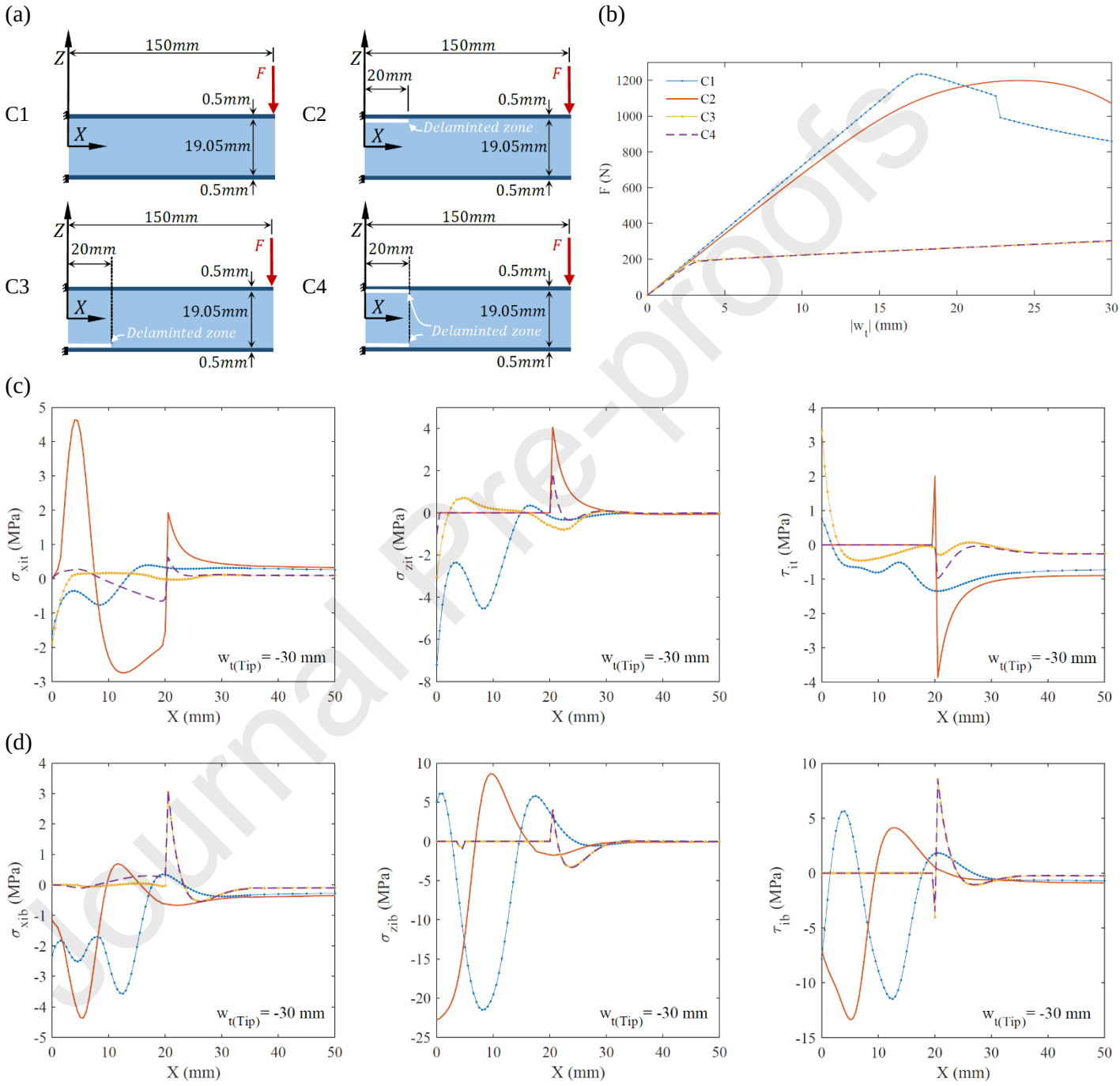

Fig. 7. Geometry and numerical results obtained for cantilever sandwich beams with upper or/and lower end delamination under the load applied on the upper face sheet at the tip point: (a) geometry; (b) load versus tip displacement; (c) interfacial axial normal stress at core-upper face interfaces and shear stress in core; (d) interfacial axial normal stress at core-lower face interfaces and shear stress in core.

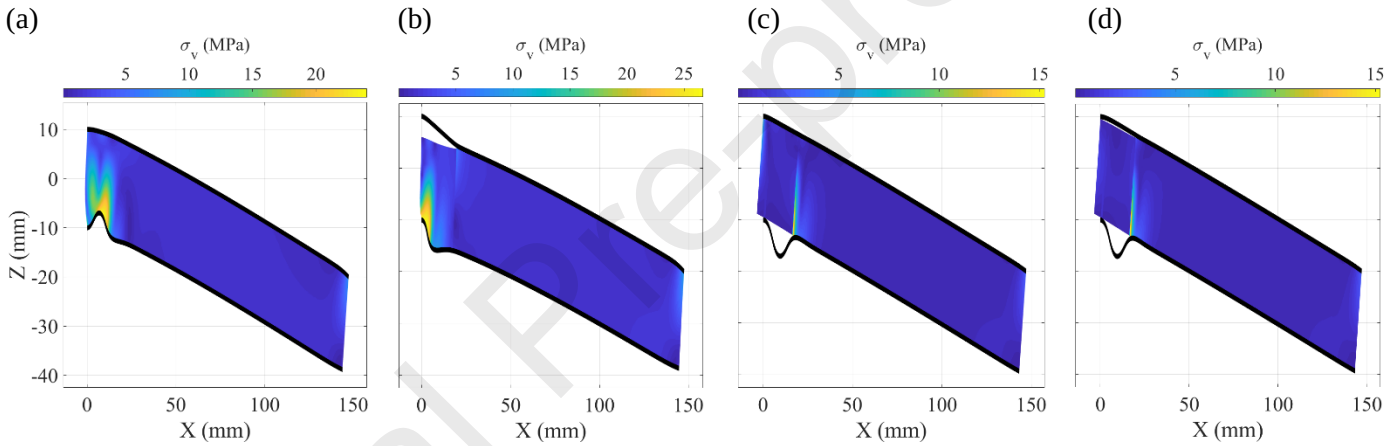

Fig. 8. Final configuration and von-Mises stress distribution of the sandwich beam C1-C4 as depicted in Fig. 7a at the end of loading.

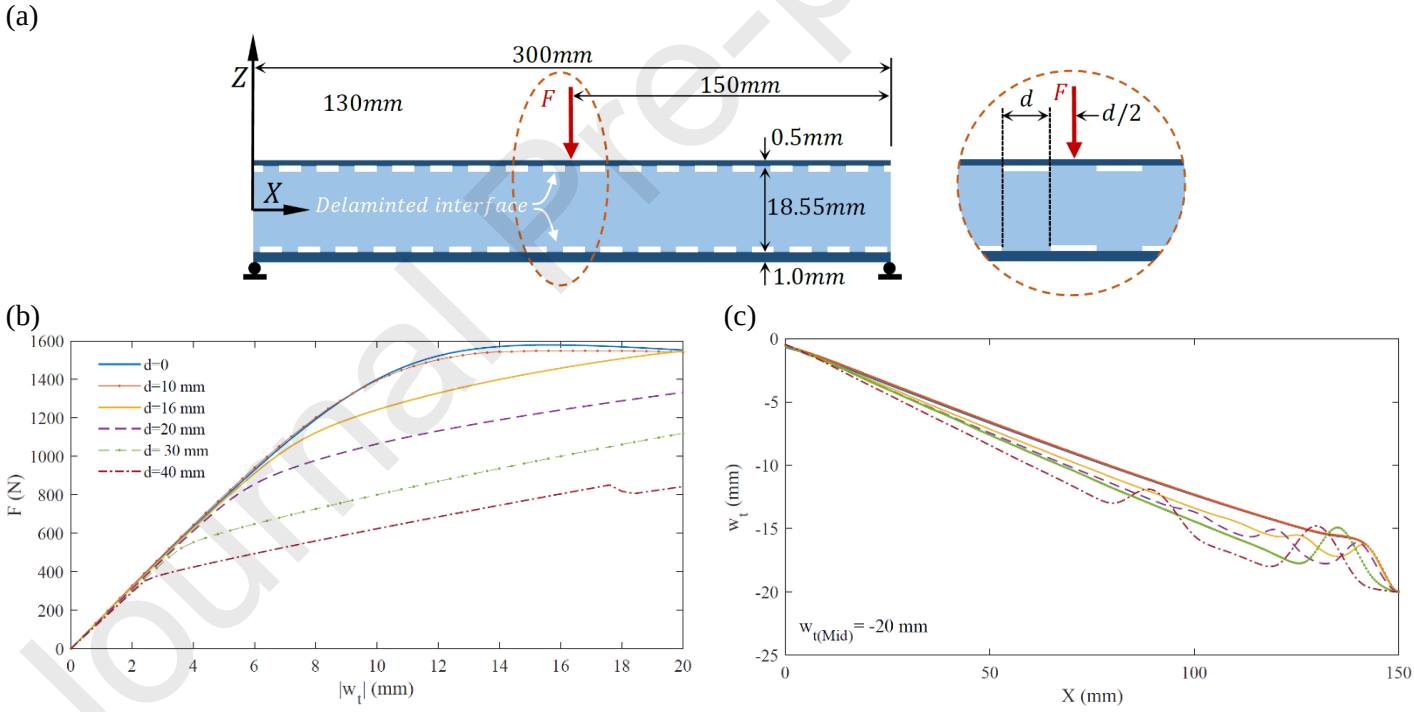

Fig. 9. Geometry and numerical results obtained for clamped sandwich beams with upper continuous delaminations under a point load applied on the upper face sheet at the mid span: (a) geometry; (b) load versus top-mid-span displacement; (c) vertical displacements in top face sheet along half-length of the beam for various values of *d*.

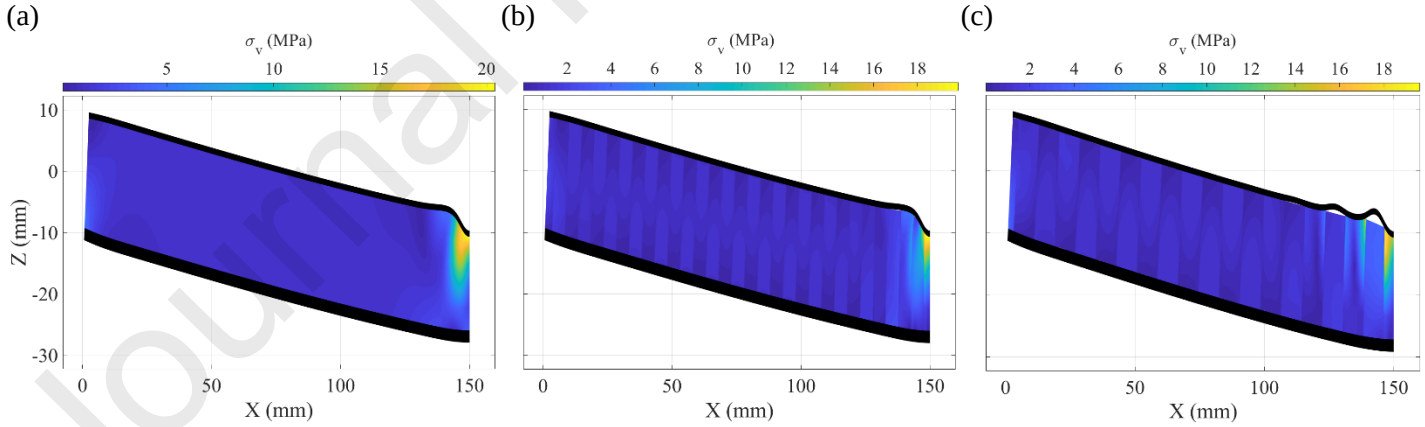

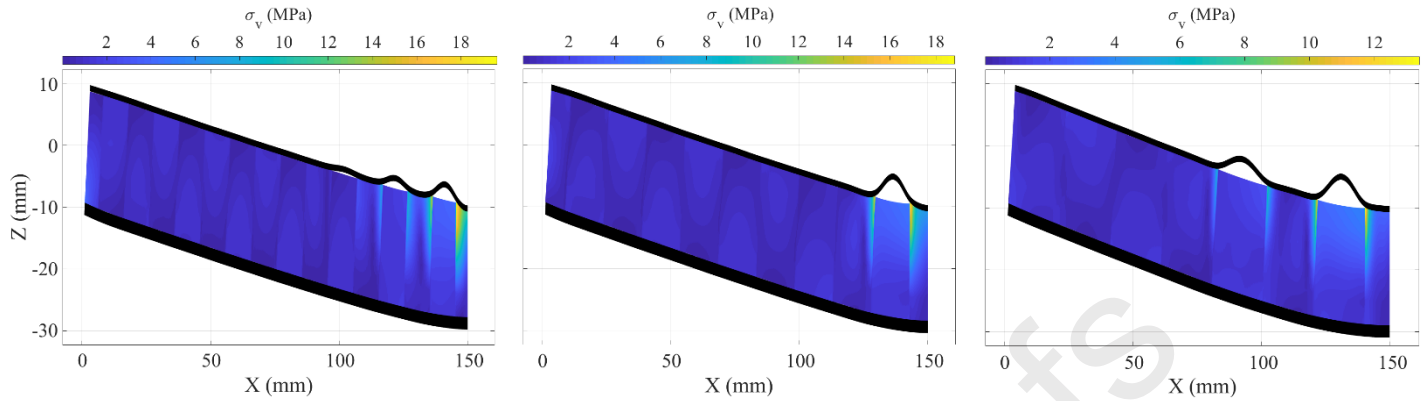

Fig. 10. Configuration and distribution of von-Misses stress of the core related to Fig. 9a for (d) $d = 0$; (e) $d = 10\ mm$; (f) $d = 16\ mm$; (g) $d = 20\ mm$; (h) $d = 30\ mm$; and (i) $d = 40\ mm$.

Author Statement

Conceptualization and modeling: A.R.D.;

Data collection and analysis: A.R.D. and M.B.;

Writing & editing: A.R.D. and M.B.;

All authors have read and approved the current version of the paper and the order of authors listed in the paper.